

## Article

# Mechanistic Study in Gold Nanoparticle Synthesis through Microchip Laser Ablation in Organic Solvents

Barana Sandakelum Hettiarachchi <sup>1</sup>, Yusuke Takaoka <sup>2</sup>, Yuta Uetake <sup>1,3</sup>, Yumi Yakiyama <sup>1,3,\*</sup>, Hiroshi Y. Yoshikawa <sup>2</sup>, Mihoko Maruyama <sup>4</sup> and Hidehiro Sakurai <sup>1,3,\*</sup>

<sup>1</sup> Division of Applied Chemistry, Graduate School of Engineering, Osaka University, 2-1 Yamada-oka, Suita, Osaka 565-0871, Japan; barana@chem.eng.osaka-u.ac.jp (B.S.H.); uetake@chem.eng.osaka-u.ac.jp (Y.U.)

<sup>2</sup> Division of Applied Physics, Graduate School of Engineering, Osaka University, 2-1 Yamada-oka, Suita, Osaka 565-0871, Japan; takaoka@mp.ap.eng.osaka-u.ac.jp (Y.T.); hiroshi@ap.eng.osaka-u.ac.jp (H.Y.Y.)

<sup>3</sup> Innovative Catalysis Science Division, Institute for Open and Transdisciplinary Research Initiatives (ICS-OTRI), Osaka University, 2-1 Yamada-oka, Suita, Osaka 565-0871, Japan

<sup>4</sup> Division of Electrical, Electronic and Infocommunications Engineering, Graduate School of Engineering, Osaka University, 2-1 Yamada-oka, Suita, Osaka 565-0871, Japan; maruyama@eei.eng.osaka-u.ac.jp

\* Correspondence: yakiyama@chem.eng.osaka-u.ac.jp (Y.Y.); hsakurai@chem.eng.osaka-u.ac.jp (H.S.); Tel.: +81-6-6879-4592 (Y.Y.); +81-6-6879-4591 (H.S.)

**Abstract:** The utilization of pulsed laser ablation in liquids (PLALs) for preparing gold nanoparticles (Au NPs) in organic solvents holds immense potential across diverse applications. This study introduces a compact and low-power microchip laser (MCL) system (average power 50 mW; pulse energy 0.5 mJ). Due to its compactness, an MCL is advantageous for easy manipulation in organic laboratories during the production of metal nanoparticles (NPs) for research and development purposes. In this research, poly(*N*-vinyl-2-pyrrolidone) (PVP) is used as a stabilizing agent for the preparation of Au NPs in organic solvents (CH<sub>2</sub>Cl<sub>2</sub>, CHCl<sub>3</sub>, 2-PrOH, MeCN, DMF, EtOH, NMP, and DMSO). Our experimental results demonstrate that the particle size remains consistent across all the organic solvents. This study explores the productivity of Au NPs in different organic solvents, revealing the necessity of multiple laser pulses to generate Au NPs successfully. This phenomenon, known as the ‘incubation effect,’ is linked to the lower pulse energy in the experimental condition and the thermal conductivity of the solvents. The findings emphasize the crucial role of solvent properties in determining the Au NPs productivity in PLAL.

**Keywords:** pulsed laser ablation in liquids; microchip laser; gold nanoparticles; organic solvents; thermal conductivity



**Citation:** Hettiarachchi, B.S.; Takaoka, Y.; Uetake, Y.; Yakiyama, Y.; Yoshikawa, H.Y.; Maruyama, M.; Sakurai, H. Mechanistic Study in Gold Nanoparticle Synthesis through Microchip Laser Ablation in Organic Solvents. *Metals* **2024**, *14*, 155. <https://doi.org/10.3390/met14020155>

Academic Editor: Gregory Guisbiers

Received: 31 December 2023

Revised: 22 January 2024

Accepted: 25 January 2024

Published: 27 January 2024



**Copyright:** © 2024 by the authors. Licensee MDPI, Basel, Switzerland. This article is an open access article distributed under the terms and conditions of the Creative Commons Attribution (CC BY) license (<https://creativecommons.org/licenses/by/4.0/>).

## 1. Introduction

Gold nanoparticles (Au NPs) have gained considerable attention due to their exceptional ability to strongly absorb electromagnetic waves in the visible spectrum through surface plasmon resonance. This unique property, coupled with their ability to stay evenly dispersed in the presence of a matrix, has made them a subject of great interest in a wide range of areas, such as sensors, electronics, medical treatments, solar cells, drug delivery, and catalysts [1,2]. In this specific context, pulsed laser ablation in liquids (PLALs), a physical metal nanoparticles (NPs) generation method, has attracted attention in the recent past and employs a pulsed laser focused on a bulk target immersed in a liquid medium to ablate material [3–5]. This technique offers several advantages over conventional metal NP preparation methods, such as the chemical reduction method, in terms of the absence of reducing agents, operational simplicity, high purity devoid of purification steps, and ambient processing conditions, which enable the easy utilization of the NPs even in biologic and medical applications. The PLAL method also allows the use of various kinds of organic solvents, such as DMSO, DMF, MeCN, THF, acetone, and even less polar alkanes, as well

as simple aromatics such as toluene, etc. [6]. The usage of organic solvents affords unique results depending on their physical properties, which cannot be observed in the aqueous condition. One of the prominent features of PLALs in organic solvents is that they often exhibit the formation of carbon-coated NPs [7,8]. This keeps particle sizes small and works as the substrate for further functionalization [9]. In addition, Amendola et al. showed that the size and aggregation of the nanoparticles can be easily manipulated by changing the laser parameters in the ablation process using DMSO, MeCN, and THF [10]. Giorgetti et al. demonstrated that Au NPs exhibit enhanced stability and fluorescent properties when ablated in acetone, in contrast to those obtained in water [11]. Compagnini et al. have shown the possibility of surface functionalization with alkanethiols during ablation in alkane/alkane-thiol solutions [12]. In this study, we introduced the diode laser-pumped microchip laser (MCL) system, pioneered by Taira et al., for PLAL (Figure 1) [13,14]. This MCL device offers portability due to its short cavity length of under 10 mm, making it well suited for standard organic synthesis laboratories and realizing the direct application of so-formed metal NPs to further the catalytic reaction via in situ operations. In addition, MCLs with a pulse duration of 0.9 ns exhibit optimal efficiency compared to those with plasma pulse durations of a few ps and >5 ns. This is because of the shielding effect of the laser beam by the ablation plume and cavitation bubble, which occurs between 1 and 5 ns after the pulse, resulting in minimal pulse energy losses for PLAL [15]. More importantly, the low repetition rate of our MCL (100 Hz) prevents heat accumulation caused by pulse overlapping, allowing the use of various organic solvents for the preparation of metal NPs without concerns about flammability. In our prior experiment, we employed the MCL device to successfully generate Au NPs in aqueous poly(*N*-vinyl-2-pyrrolidone) (PVP) solutions and found that the MCL shows comparable performance with the high-power laser [16]. With this background, here we present a comprehensive study of the preparation of Au NPs within various organic solvents ( $\text{CH}_2\text{Cl}_2$ ,  $\text{CHCl}_3$ , 2-PrOH, MeCN, DMF, EtOH, NMP, and DMSO), which are often used in organic synthesis, employing PVP as a stabilizing agent. Employing low pulse energy in the experimental setup, along with the thermal conductivity of the solvents, resulted in the requirement of multiple laser pulses for the successful production of Au NPs. This phenomenon, commonly referred to as the ‘incubation effect’, highlights the significance of considering both experimental parameters and solvent characteristics in the precise synthesis of NPs.

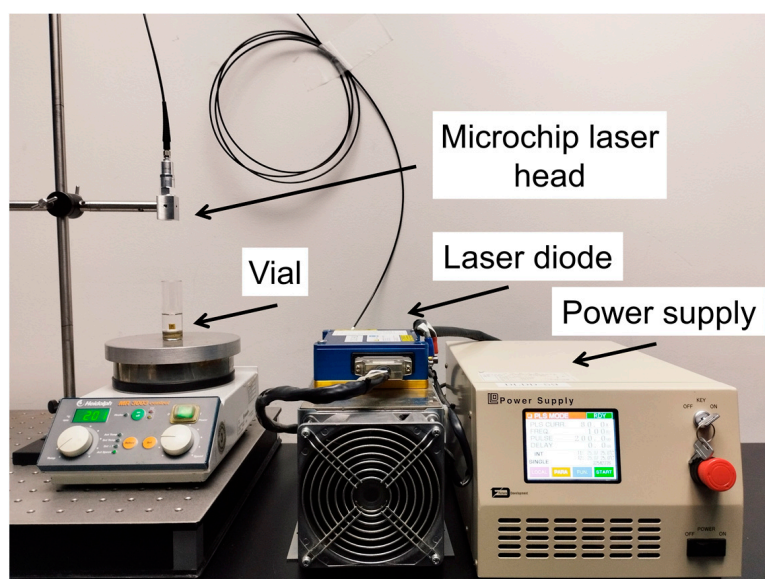


**Figure 1.** Configuration and components of the microchip laser system.

## 2. Materials and Methods

**General:** Commercially purchased reagents were utilized without additional purification unless specifically stated. Ultrapure water ( $18.2 \Omega \cdot \text{cm}^{-1}$ ) was prepared using an Organo Puric- $\omega$  water purification system. Transmission Electron Microscopy (TEM) images were captured using a JEM-2100 electron microscope (JEOL, Tokyo, Japan) (operating at 200 kV acceleration voltage). A holey carbon support film-coated Cu microgrid U1003 (EM Japan, Tokyo, Japan) was employed. Prior to use, the TEM grid underwent hydrophilic treatment through glow discharge irradiation. Image-J software (version 1.52a) was employed to analyze the acquired TEM images, with the mean diameter and standard deviation values derived from measurements of 300 particles on average. Inductively Coupled Plasma Atomic Emission Spectroscopy (ICP-AES) analysis was performed using an ICPS-8100 instrument (Shimadzu, Kyoto, Japan). Viscosity measurements were carried out using the HAAKE RheoStress 6000 instrument (Thermo Scientific, Waltham, MA, USA). Measurements were conducted at a shear rate of  $1000 \text{ s}^{-1}$  and a temperature of  $25 \text{ }^\circ\text{C}$ . As no significant viscosity discrepancies were observed between pre- and post-PLAL conditions, all viscosity measurements were acquired post-PLAL.

**MCL Specification:** The MCL comprised a monolithic Nd:YAG/Cr<sup>4+</sup>:YAG ceramic with a dimension of  $3 \times 3 \times 10 \text{ mm}^3$ . The Nd-doping rate and the initial transmittance of Cr<sup>4+</sup>:YAG were 1.1 at.% and 30%, respectively. The input surface was dual-coated for anti-reflection (AR) at 808 nm for the end pump and high reflection (HR) at 1064 nm for laser oscillation. The output surface was 50% partial reflection (PR) coated for the same laser wavelength. The monolithic ceramics were set in a metal module with two lenses for the fiber-coupled pump. The MCL generated laser pulses with a  $>0.5 \text{ mW}$  peak power (pulse energy of 0.5 mJ and a pulse duration of 900 ps) at 100 Hz (average power of 50 mW) without active cooling.

**General PLAL method:** A gold target ( $>99.99\%$ ,  $5 \times 15 \text{ mm}$ ) was cleaned with ultrasonication in acetone for 5 min and rinsed with deionized water. The target was fixed on a custom-made holder (PEEK) equipped with a magnetic stir bar, and then this was placed at the bottom of a Pyrex<sup>®</sup> vessel ( $30 \times 80 \text{ mm}$ ). The appropriate number of zirconia beads ( $\varphi 6 \text{ mm}$ ) were placed between the vessel and the holder to prevent the axis of rotation from moving. To this vessel, 15 mL of 0.1 M poly (*N*-vinyl-2-pyrrolidone) (PVP (K-15 (10 kDa)))/organic solvent ( $\text{CH}_2\text{Cl}_2$ ,  $\text{CHCl}_3$ , 2-PrOH, MeCN, DMF, EtOH, NMP, and DMSO) was applied. Afterward, the pulsed laser was irradiated on the gold target at room temperature for 60 min while the Au target rotated at 200 rpm. A parallel experiment was also conducted without PVP in each organic solvent. Consistent laser parameters were applied across all experiments: wavelength, 1064 nm; pulse energy, 1.8 mJ; pulse duration, 900 ps; average laser power, 180 mW; repetition rate, 100 Hz. The resulting Au NPs were subjected to subsequent analyses. To change the pulse energy, we changed the applied current.

**Real-time monitoring using a high-speed camera:** A high-speed camera (HPV-2, Shimadzu Corporation,  $312 \times 260$  pixels, maximum frame rate = 1000 kfps) was synchronized with the MCL via a function generator WF1943 (Wave Factory, Yokohama, Japan). One hundred images were recorded for MCL ablation using 250  $\mu\text{s}$  frame intervals for organic solutions ( $\text{CH}_2\text{Cl}_2$ ,  $\text{CHCl}_3$ , 2PrOH, MeCN, DMF, EtOH, NMP, and DMSO) containing PVP K-15 at a concentration of 0.1 M. A parallel experiment was also conducted without PVP. The gold sample was observed through an objective lens  $2\times$ , NA, 0.06 (Olympus, Tokyo, Japan) in front of the camera. An LED light source DC20 (THORLABS, Newton, NJ, USA) was used for illumination. The liquid level was set to be 5 mm above the gold surface. The laser beam was directly focused on the target surface. The average spot size at the laser focus ( $130 \pm 6 \mu\text{m}$ ) was measured by ablating black ink on a glass substrate in air, which corresponds to a nominal laser fluence of  $13.5 \text{ J/cm}^2$  (several times larger than ablation threshold fluences of  $2.1 \text{ J/cm}^2$ ). The detailed setting is depicted in Figure S1.

### 3. Results and Discussion

In most research studies, aqueous solutions are commonly used for laser ablation in liquids. At the same time, there have been investigations into organic liquids to produce colloidal NPs. The presence of an organic solvent in laser irradiation significantly affects the product formation, causing the generation of graphite shells [17], carbides [18], and nitrides [19]. Additionally, the physical properties of the chosen solvent, such as its density [20], viscosity [21], polarity [22], and thermal reactivity [23], also influence the outcome of the pulsed laser ablation process. The presence of another material in the system also affects the ablation event. For example, PVP is a commonly utilized polymer as a stabilizing agent for metal colloids, especially in the chemical reduction method, and its concentration and chain length significantly affect not only the resulting particle size but also further catalytic reaction efficiency [24–30]. It has also been used in PLAL [31,32] and affects the final particle size of Ag NPs (5–10 nm in  $\text{CHCl}_3$ , ~200 nm in toluene) simply due to the solubility difference [33]. Other parameters, such as the molecular weight and the concentration, must also be considered in the PLAL case. However, our previous report of PLAL using MCL in an aqueous solution has already confirmed that neither the molecular weight nor the concentration of PVP affect the size of the generated Au NPs [16]. Thus, this paper investigated how the resulting particle size and Au productivity change depending on the solvent employed in the presence of PVP K-15.

The present PLAL experiments with our MCL system (1.8 mJ/pulse, 100 Hz) were performed in a total of eight organic solvents:  $\text{CH}_2\text{Cl}_2$ ,  $\text{CHCl}_3$ , 2-PrOH, MeCN, DMF, EtOH, NMP, and DMSO. All the systems successfully worked in producing Au NPs, and the particle size confirmed by TEM measurement exhibited consistency across all trials, ranging from 3 to 4 nm (Table 1 and Figure S2). These results indicated that variations in organic solvents do not significantly impact particle size determination. This observed particle size aligned with our previous experiments that were conducted using aqueous PVP solutions, giving 3 to 4 nm size Au NPs [16]. The phenomenon is our MCL system's characteristics, specifically its low pulse energy and low repetition rate (100 Hz). Such conditions afford tiny and shorter-lived cavitation bubbles that cannot be detected by video monitoring, providing limited space for the nucleation and growth of NPs. When considering the role of PVP, it is a polar molecule, is nicely soluble in all the organic solvents utilized here, and has no solubility effect on the size of the generated Au NPs. Instead, it was mainly effective for quenching the growth of NPs after cavitation bubble collapse.

**Table 1.** PLAL on gold target in organic solvents with PVP (K-15).

Solvent <sup>a</sup>	Particle Size (nm)	Au Productivity ( $\mu\text{g}/\text{h}$ )	Viscosity ( $\text{mPa}\cdot\text{s}$ )	Thermal Conductivity ( $\text{W}/\text{m}\cdot\text{K}$ ) [34,35]	Required Number of the Pulse
$\text{CH}_2\text{Cl}_2$	$3.2 \pm 0.7$	79.3	$0.68 \pm 0.02$	0.13	1
$\text{CHCl}_3$	$3.5 \pm 1.0$	109.1	$0.67 \pm 0.02$	0.12	1
2-PrOH	$4.4 \pm 1.1$	134.7	$2.92 \pm 0.02$	0.16	3
MeCN	$3.5 \pm 0.7$	147.5	$0.45 \pm 0.02$	0.15	4
DMF	$3.4 \pm 0.8$	155.2	$1.12 \pm 0.02$	0.16	4
EtOH	$3.4 \pm 0.8$	166.8	$1.81 \pm 0.02$	0.17	6
NMP	$3.3 \pm 0.4$	168.6	$2.16 \pm 0.02$	0.18	6
DMSO	$3.0 \pm 0.8$	173.1	$2.72 \pm 0.02$	0.20	6

<sup>a</sup> All solvent amounts were fixed at 15 mL. The concentration of PVP (K-15) was 0.1 M.

Meanwhile, the investigation of ablation efficiency indicated variations in the AuNP yield, especially between halogenated solvents ( $\text{CH}_2\text{Cl}_2$  and  $\text{CHCl}_3$ ) and the others (Table 1). There are various possible factors responsible for the ablation efficiency of PLAL. Our previous report showed that ablation efficiency using the present MCL depended on solution viscosity, which could be controlled by the concentration and chain length of PVPs [16]. This dependency arises from the slow diffusion of laser-induced tiny gas bubbles in high-viscosity media, which shields the subsequent laser pulse energy and results in low ablation efficiency. The viscosity effect was also confirmed in PLAL using water, acetone, and ethylene glycol [36]. In this context, we first focused on the correlation between the yield of Au NPs and the viscosity of organic solvents in the presence of PVP. However, no clear relationship was confirmed (Table 1, Figure S3), which indicated that the yield of Au NPs was more affected by the type of organic solvent than the solution viscosity. Then, we next considered other possible factors affecting micro gas bubble formation, such as solvent pyrolysis activation energy and vaporization enthalpy. It is reported that gas bubble formation is linearly correlated with the activation energy of solvent pyrolysis [37]. This pyrolysis occurs at high temperatures and pressures, resulting in the generation of carbon products like a carbon shell. However, in our analysis, we did not observe any carbon shell formation on the surface of Au NPs, which was probably due to the low laser power of the MCL system, and therefore, we assume that the activation energy for pyrolysis did not significantly contribute to ablation efficiency. It is also known that a solvent with low vaporization enthalpy leads to decomposition, forming gas bubbles that result in laser pulse shielding effects, subsequently decreasing the laser ablation efficiency [37]. In our experimental conditions,  $\text{CH}_2\text{Cl}_2$  and  $\text{CHCl}_3$  possess lower vaporization enthalpy than the others ( $\text{CH}_2\text{Cl}_2$ : 28.5 kJ/mol,  $\text{CHCl}_3$ : 30.5 kJ/mol, 2-PrOH: 46.0 kJ/mol, MeCN: 33.8 kJ/mol, DMF: 46.7 kJ/mol, Ethanol: 42.3 kJ/mol, NMP: 55.3 kJ/mol, DMSO: 52.9 kJ/mol) [38]. This lower vaporization enthalpy of halogenated solvents probably generated a more significant amount of gas bubbles, resulting in lower laser ablation efficiency, as shown in Table S1. Meanwhile, the same experiment without PVP exhibited a significant decrease in yield in  $\text{CH}_2\text{Cl}_2$  and  $\text{CHCl}_3$  (40–70  $\mu\text{g}/\text{h}$ ), while the other solvents showed only slight deviations (9–14  $\mu\text{g}/\text{h}$ ) (Table S1 and Figure 2a). It has been reported that PVP increases the heat capacity of the system to reduce gas bubble formation [39]. Our experimental result indicated that the above PVP effect was prominent when the vaporization enthalpy was low, while it did not affect much in higher vaporization enthalpy solvents.

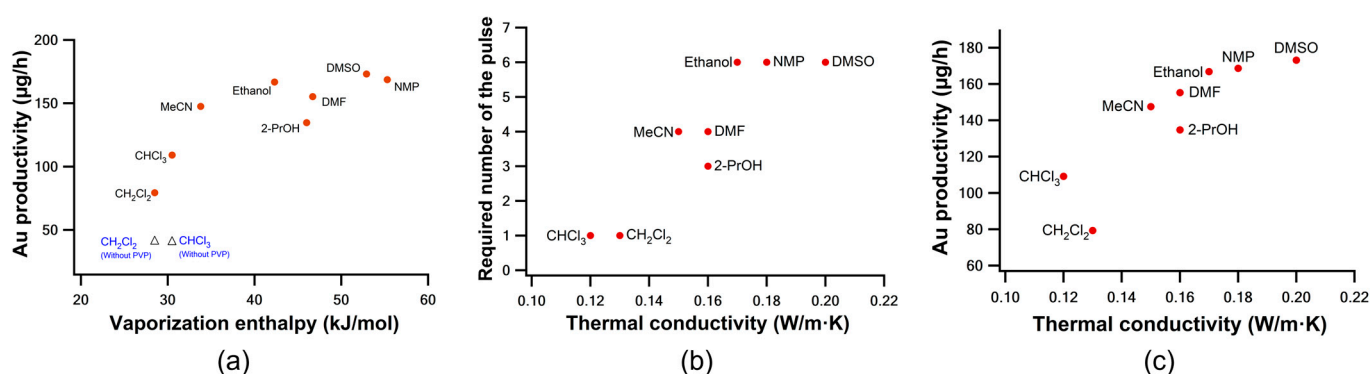


**Figure 2.** (a) Plot of the ablated Au amount versus vaporization enthalpy (red circles represent all of the solvents in the presence of PVP, and black triangles represent the results using  $\text{CH}_2\text{Cl}_2$  and  $\text{CHCl}_3$  in the absence of PVP); (b) the required number of the pulse versus thermal conductivity in the presence of PVP; and (c) ablated Au amount versus vaporization enthalpy in the presence of PVP.

To gain insight into the underlying mechanism behind ablation efficiency in MCL-based PLAL using organic solvents in the presence of PVP K-15, the ablation process of Au NPs was monitored in real-time using a high-speed camera, capturing images at a frequency of 250  $\mu\text{s}$  per frame during the initial laser ablation (Figure 3 and Videos S1–S8). As seen in our previous work, the cavitation bubble could not be observed in high-speed camera experiments in the current work [16]. Although cavitation bubble formation almost certainly occurred in the present system, the smaller size of the cavitation bubble due to the present MCL spec and the low temporal resolution may be the reason for the challenge of observing the formation of cavitation bubbles in the current system. As shown in Figure 3 and Videos S1–S8, the generation of Au NPs required different numbers of laser pulses in various organic solvents. Single pulses did not lead to NP production in all the cases. To cause the ablation phenomenon, high enough energy localization at the target surface should occur, which is generally suppressed somewhat by the reflection of the laser beam on the target surface and heat energy diffusing into the target [40]. However, in the present case, it was simply rationalized by the low induced energy, which did not reach the ablation threshold due to the low pulse energy. The other possible phenomenon to be considered in this observation may be the heat diffusion from the bulk gold surface to the surrounding solvent. One important parameter to determine to control the superheated degree of the molten surface is the thermal conductivity of the surrounding solvent. As shown in Figure 2b and Table 1, our experimental results demonstrated a linear-like correlation between the thermal conductivity of organic solvents [34,35] and the required number of laser pulses to achieve proper ablation. This is associated with an incubation behavior of the ablation threshold fluence of the target, i.e., the decreasing ablation threshold with an increasing number of pulses per spot by the formation of a rougher target surface (Figure 4) [40,41]. The lower thermal conductivity of  $\text{CH}_2\text{Cl}_2$  and  $\text{CHCl}_3$  than that of the other solvents suppressed heat diffusion effectively from the gold target surface to the outer media, enabling a single laser pulse to be sufficient to vaporize and ablate the bulk gold target [42]. In contrast, the other solvents with more than  $0.15 \text{ W/m}\cdot\text{K}$  thermal conductivity allowed more considerable heat diffusion from the bulk gold target surface, requiring multiple laser pulses to start ablation.

Our experimental results demonstrated that vaporization enthalpy affected the gas bubble formation during the ablation and thermal conductivity determined the number of required laser pulses for Au NPs ablation with inducing target surface roughness, which were also confirmed in the previous works. Noteworthy is that the rougher surface affords better ablation efficiency per pulse [40], and indeed, the plot between the thermal conductivity of each solvent and the Au productivity showed a linear-like curve (Figure 2c). Although further consideration of the effect of solvent density and direct monitoring of the target surface in each case are needed, this result seemed reasonable since the system requiring several pulses for target ablation formed a rougher surface than the case with single or double laser shots. The formation of gas bubbles during the ablation process, influenced by the vaporization enthalpy of the solvent, was also a considerable factor, and the effect was also confirmed in Figure 2a. However, this shielding effect was less pronounced when the solvent had a high enough vaporization energy ( $>33 \text{ kJ/mol}$  (MeCN)). Our experimental observation suggested that the solvent thermal conductivity was considered a primary factor influencing ablation efficiency and the vaporization enthalpy as a cofactor, especially in the absence of polymers in low-vaporization solvents.

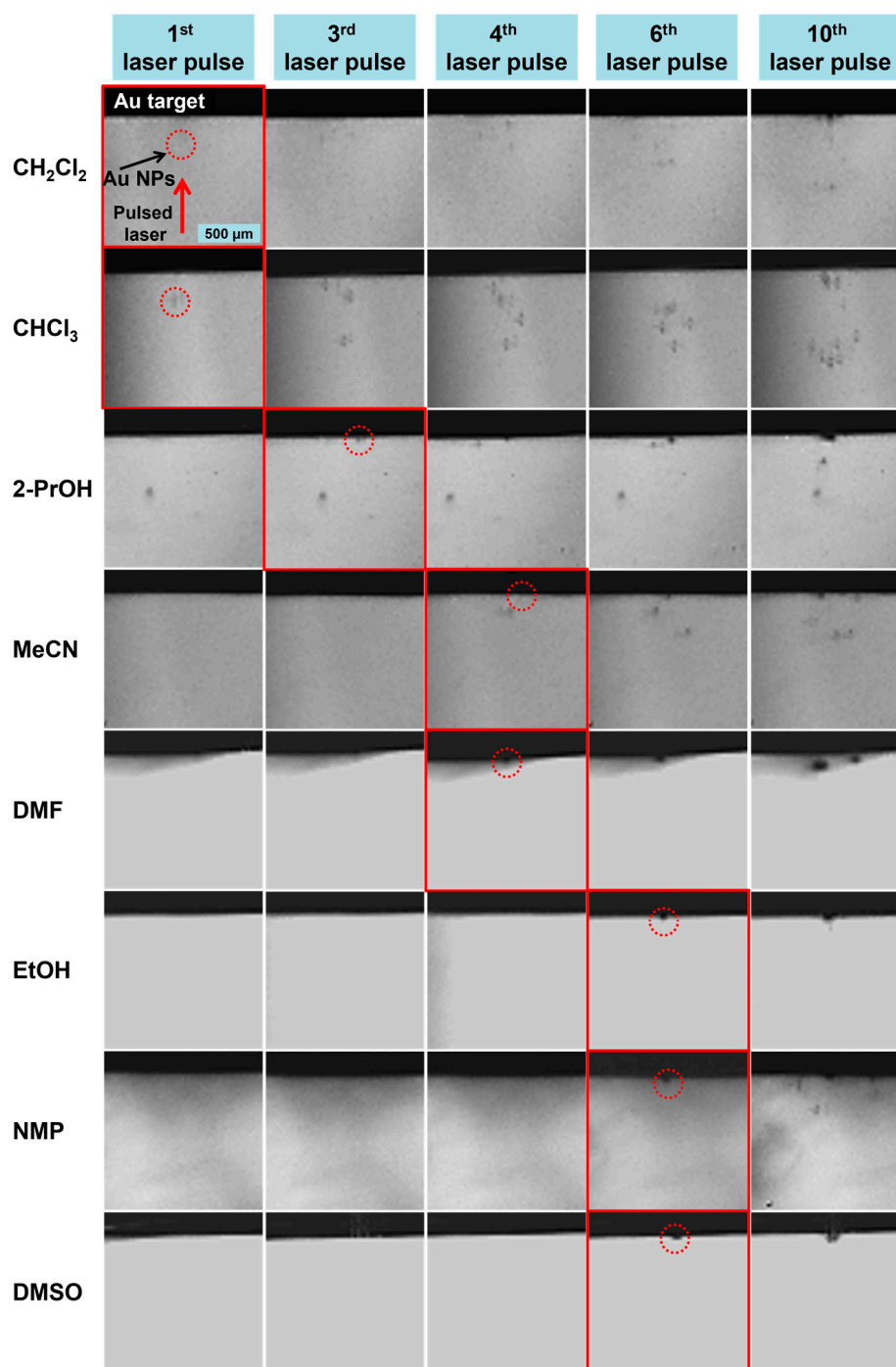
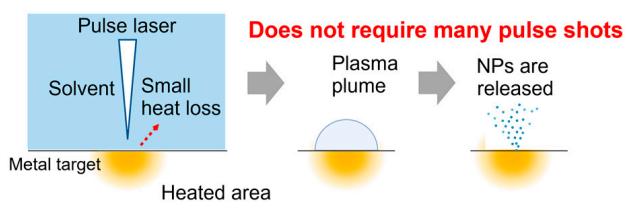


**Figure 3.** Selected videographic images of Au NPs ablation in different organic solvents in the presence of PVP K-15 (0.1 M) by MCL. Au NPs generation in each solvent started after different numbers of laser pulses (highlighted by a red square). In each solvent, the ejected Au NPs from the corresponding laser pulse were indicated by a red circle. The experimental setup depicted in Figure S1 involved a pulsed laser, marked by a red arrow, which was irradiated vertically from top to bottom. However, the resulting image captured by the camera was inverted, showing the opposite direction. In the 2-PrOH sample, previously generated metal NPs are present as contamination due to several attempts to position and achieve precise imaging for accurate ablation.

## (a) In low thermal conductivity solvent



## (b) In high thermal conductivity solvents

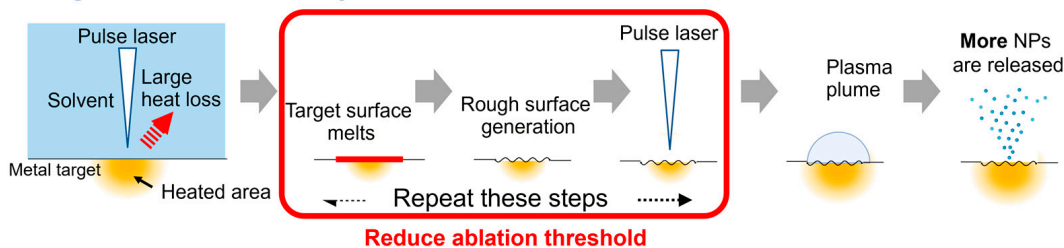


**Figure 4.** Schematic representation of the laser ablation mechanism with consideration of the incubation effect in (a) low thermal conductivity solvents and (b) high thermal conductivity solvents.

#### 4. Conclusions

This study successfully demonstrated the preparation of Au NPs in various organic solvents using PLAL with an MCL system. Throughout the study, laser irradiation consistently produced small particle sizes of Au NPs in different organic solvents in the presence of PVP. Furthermore, the study investigated the influence of various organic solvents on the ablation efficiency of Au NPs. The choice of solvent significantly affected the number of laser pulses required for NP generation. This phenomenon was attributed to the incubation effect and was correlated with both the applied laser energy and the thermal conductivity of the solvent. Solvents with high thermal conductivity demonstrated enhanced ablation efficiency, while vaporization enthalpy was also found to be a cofactor, especially in the absence of polymers in low-vaporization solvents. This innovative approach overcomes the limitations of high-power laser systems when handling flammable organic solvents, making it a promising method for advanced NP preparation. Our findings elucidate the intricate factors influencing PLAL in non-aqueous media and offer valuable insights for optimizing NP synthesis processes in various solvent environments.

**Supplementary Materials:** The following supporting information can be downloaded at <https://www.mdpi.com/article/10.3390/met14020155/s1>. Figure S1: Experimental setup for monitoring the bubble formation with the aid of videography; Figure S2: TEM images of Au: PVP (K-15) in organic solvents.; Figure S3: Viscosity effect on Au NPs productivity.; Table S1: Ablated total Au amount in the absence of PVP; Video S1: CH<sub>2</sub>Cl<sub>2</sub>; Video S2: CHCl<sub>3</sub>; Video S3: 2-PrOH; Video S4: MeCN; Video S5: DMF; Video S6: EtOH; Video S7: NMP; Video S8: DMSO.

**Author Contributions:** Conceptualization, Y.Y. and H.S.; validation, B.S.H., Y.Y. and H.S.; formal analysis, B.S.H.; investigation, B.S.H., Y.T. and Y.U.; resources, H.Y.Y. and M.M.; data curation, B.S.H., H.Y.Y., Y.U. and Y.Y.; writing—original draft preparation, B.S.H.; writing—review and editing, Y.Y., H.Y.Y., Y.T., M.M. and H.S.; visualization, Y.Y.; supervision, Y.Y. and H.S.; project administration, H.S.; funding acquisition, Y.Y. and H.S. All authors have read and agreed to the published version of the manuscript.

**Funding:** This study was supported by JSPS KAKENHI (JP19K22187). Y.Y. acknowledges the Amada Foundation for the Promotion of Science and Engineering for financial support. B.S.H. thanks the Japan International Cooperation Agency (JICA) and the Otsuka Toshimi Scholarship Foundation for kindly providing scholarships.

**Data Availability Statement:** The original contributions presented in the study are included in the article and supplementary material, further inquiries can be directed to the corresponding authors.

**Acknowledgments:** We thank Taka-aki Asoh (Tokyo University of Science) and Satoshi Seino (Osaka University) for their support of viscosity and TEM measurements, respectively. We thank Hwan Hong Lim (Institute for Molecular Science (IMS)) and Takunori Taira (IMS and RIKEN) for lending and the technical assistance of MCL.

**Conflicts of Interest:** The authors declare no conflicts of interest.

## References

1. Li, N.; Zhao, P.; Astruc, D. Anisotropic gold nanoparticles: Synthesis, properties, applications, and toxicity. *Angew. Chem. Int. Ed.* **2014**, *53*, 1756–1789. [[CrossRef](#)] [[PubMed](#)]
2. Zhang, J.; Mou, L.; Jiang, X. Surface chemistry of gold nanoparticles for health-related applications. *Chem. Sci.* **2020**, *11*, 923–936. [[CrossRef](#)] [[PubMed](#)]
3. Zhang, D.; Li, Z.; Sugioka, K. Laser ablation in liquids for nanomaterial synthesis: Diversities of targets and liquids. *J. Phys. Photonics* **2021**, *3*, 042002. [[CrossRef](#)]
4. Zhang, D.; Gökce, B.; Barcikowski, S. Laser synthesis and processing of colloids: Fundamentals and applications. *Chem. Rev.* **2017**, *5*, 3990–4103. [[CrossRef](#)] [[PubMed](#)]
5. Theerthagiri, J.; Karuppasamy, K.; Lee, S.J. Fundamentals and comprehensive insights on pulsed laser synthesis of advanced materials for diverse photo- and electrocatalytic applications. *Light Sci. Appl.* **2022**, *11*, 250. [[CrossRef](#)] [[PubMed](#)]
6. Amendola, V.; Meneghetti, M. Laser ablation synthesis in solution and size manipulation of noble metal nanoparticles. *Phys. Chem. Chem. Phys.* **2009**, *11*, 3805–3821. [[CrossRef](#)] [[PubMed](#)]
7. Amendola, V.; Polizzi, S.; Meneghetti, M. Free silver nanoparticles synthesized by laser ablation in organic solvents and their easy functionalization. *Langmuir* **2007**, *23*, 6766–6770. [[CrossRef](#)]
8. Zhang, D.; Zhang, C.; Liu, J.; Cen, Q.; Zhu, X.; Liang, C. Carbon-Encapsulated Metal/Metal Carbide/Metal Oxide Core-Shell Nanostructures Generated by Laser Ablation of Metals in Organic Solvents. *ACS Appl. Nano Mater.* **2019**, *2*, 28–39. [[CrossRef](#)]
9. Grass, R.N.; Athanassio, E.K.; Stark, W.J. Covalently Functionalized Cobalt Nanoparticles as a Platform for Magnetic Separations in Organic Synthesis. *Angew. Chem. Int. Ed.* **2007**, *46*, 4909–4912. [[CrossRef](#)]
10. Amendola, V.; Polizzi, S.; Meneghetti, M.; Amendola, V. Laser ablation synthesis of gold nanoparticles in organic solvents. *J. Phys. Chem. B* **2006**, *110*, 7232–7237. [[CrossRef](#)]
11. Giorgetti, E.; Muniz-Miranda, M.; Marsili, P.; Scarpellini, D.; Giammanco, F. Stable gold nanoparticles obtained in pure acetone by laser ablation with different wavelengths. *J. Nanopart. Res.* **2012**, *14*, 648. [[CrossRef](#)]
12. Compagnini, G.; Scalisi, A.A.; Puglisi, O.; Spinella, C. Synthesis of gold colloids by laser ablation in thiol-alkane solutions. *J. Mater. Res.* **2004**, *19*, 2795–2798. [[CrossRef](#)]
13. Taira, T. RE<sup>3+</sup>-ion-doped YAG ceramic lasers. *IEEE J. Sel. Top. Quantum Electron.* **2007**, *13*, 798–809. [[CrossRef](#)]
14. Sakai, H.; Kan, H.; Taira, T. >1 MW peak power single-mode high-brightness passively Q-switched Nd<sup>3+</sup>:YAG microchip laser. *Opt. Express* **2008**, *16*, 19891–19899. [[CrossRef](#)]
15. Dittrich, S.; Spellaugue, M.; Barcikowski, S.; Huber, H.P.; Gökce, B. Time resolved studies reveal the origin of the unparalleled high efficiency of one nanosecond laser ablation in liquids. *Opto-Electron. Adv.* **2022**, *5*, 210053. [[CrossRef](#)]
16. Hettiarachchi, B.S.; Takaoka, Y.; Uetake, Y.; Yakiyama, Y.; Lim, H.H.; Taira, T.; Maruyama, M.; Mori, Y.; Yoshikawa, H.Y.; Sakurai, H. Uncovering gold nanoparticle synthesis using microchip laser system through pulsed laser ablation in aqueous solution. *Ind. Chem. Mater.* **2024**. [[CrossRef](#)]
17. Amendola, V.; Rizzi, G.A.; Polizzi, S.; Meneghetti, M. Synthesis of gold nanoparticles by laser ablation in toluene: quenching and recovery of the surface plasmon absorption. *J. Phys. Chem. B* **2005**, *109*, 23125–23128. [[CrossRef](#)] [[PubMed](#)]
18. Amendola, V.; Riello, P.; Meneghetti, M. Magnetic nanoparticles of iron carbide, iron oxide, iron@iron oxide, and metal iron synthesized by laser ablation in organic solvents. *J. Phys. Chem. C* **2011**, *115*, 5140–5146. [[CrossRef](#)]
19. Begildayeva, T.; Ahn, A.; Naik, S.S.; Lee, S.J.; Theerthagiri, J.; Kim, T.H.; Choi, M.Y. Facile one-pot synthesis of CuCN by pulsed laser ablation in nitrile solvents and mechanistic studies using quantum chemical calculations. *Sci. Rep.* **2021**, *11*, 14389. [[CrossRef](#)] [[PubMed](#)]
20. Long, J.; Eliceiri, M.H.; Wang, L.; Vangelatos, Z.; Ouyang, Y.; Xie, X.; Zhang, Y.; Grigoropoulos, C.P. Capturing the final stage of the collapse of cavitation bubbles generated during nanosecond laser ablation of submerged targets. *Opt. Laser Technol.* **2021**, *134*, 106647. [[CrossRef](#)]
21. Kalus, M.-R.; Lanyumba, R.; Barcikowski, S.; Gökce, B. Discrimination of ablation, shielding, and interface layer effects on the steady-state formation of persistent bubbles under liquid flow conditions during laser synthesis of colloids. *J. Flow Chem.* **2021**, *11*, 773–792. [[CrossRef](#)]
22. Forte, G.; D’Urso, L.; Fazio, E.; Patane, S.; Neri, F.; Puglisi, O.; Compagnini, G. The effects of liquid environments on the optical properties of linear carbon chains prepared by laser ablation generated plasmas. *Appl. Surf. Sci.* **2013**, *272*, 76–81. [[CrossRef](#)]
23. Rawat, R.; Tiwari, A.; Arun, N.; Rao, S.V.S.N.; Pathak, A.P.; Shadangi, Y.; Mukhopadhyay, N.K.; Rao, S.V.; Tripathi, A. Nanosecond pulsed laser ablation of Al–Cu–Fe quasicrystalline material: Effects of solvent and fluence. *J. Alloys Compd.* **2021**, *859*, 157871. [[CrossRef](#)]

24. Zhang, G.-R.; Xu, B.-Q. Surprisingly strong effect of stabilizer on the properties of Au nanoparticles and PtAu nanostructures in electrocatalysis. *Nanoscale* **2010**, *2*, 2798–2804. [[CrossRef](#)] [[PubMed](#)]
25. Tsunoyama, H.; Ichikuni, N.; Sakurai, H.; Tsukuda, T. Effect of Electronic Structures of Au Clusters Stabilized by Poly(*N*-vinyl-2-pyrrolidone) on Aerobic Oxidation Catalysis. *J. Am. Chem. Soc.* **2009**, *131*, 7086–7093. [[CrossRef](#)] [[PubMed](#)]
26. Okumura, M.; Kitagawa, Y.; Kawakami, T.; Haruta, M. Theoretical investigation of the hetero-junction effect in PVP stabilized Au<sub>13</sub> clusters. The role of PVP in their catalytic activities. *Chem. Phys. Lett.* **2008**, *459*, 133–136. [[CrossRef](#)]
27. Haesuwannakij, S.; Kimura, T.; Furutani, Y.; Okumura, K.; Kokubo, K.; Sakata, T.; Yasuda, H.; Yakiyama, Y.; Sakurai, H. The Impact of the Polymer Chain Length on the Catalytic Activity of Poly(*N*-vinyl-2-pyrrolidone)-supported Gold Nanoclusters. *Sci. Rep.* **2017**, *7*, 9579. [[CrossRef](#)]
28. Vinsen; Uetake, Y.; Sakurai, H. Selective Oxidative Hydroxylation of Arylboronic Acids by Colloidal Nanogold Catalyzed in Situ Generation of H<sub>2</sub>O<sub>2</sub> from Alcohols Under Aerobic Conditions. *Bull. Chem. Soc. Jpn.* **2020**, *93*, 299–301. [[CrossRef](#)]
29. Dhital, R.N.; Nomura, K.; Sato, Y.; Haesuwannakij, S.; Ehara, M.; Sakurai, H. Pt–Pd Nanoalloy for the Unprecedented Activation of Carbon–Fluorine Bond at Low Temperature. *Bull. Chem. Soc. Jpn.* **2020**, *93*, 1180–1185. [[CrossRef](#)]
30. Uetake, Y.; Mouri, S.; Haesuwannakij, S.; Okumura, K.; Sakurai, H. Volcano-Type Correlation between Particle Size and Catalytic Activity on Hydrodechlorination Catalyzed by AuPd Nanoalloy. *Nanoscale Adv.* **2021**, *3*, 1496–1501. [[CrossRef](#)]
31. Tsuji, T.; Thang, D.-H.; Okazaki, Y.; Nakanishi, M.; Tsuboi, Y.; Tsuji, M. Preparation of silver nanoparticles by laser ablation in polyvinylpyrrolidone solutions. *Appl. Surf. Sci.* **2008**, *254*, 5224–5230. [[CrossRef](#)]
32. Letzel, A.; Reich, S.; dos Santos Rolo, T.; Kanitz, A.; Hoppius, J.; Rack, A.; Olbinado, M.P.; Ostendorf, A.; Gökce, B.; Plech, A.; et al. Time and mechanism of nanoparticle functionalization by macromolecular ligands during pulsed laser ablation in liquids. *Langmuir* **2019**, *35*, 3038–3047. [[CrossRef](#)] [[PubMed](#)]
33. Kassavetis, S.; Kaziannis, S.; Pliatsikas, N.; Avgeropoulos, A.; Karantzalis, A.E.; Kosmidis, C.; Lidorikis, E.; Patsalas, P. Formation of plasmonic colloidal silver for flexible and printed electronics using laser ablation. *Appl. Surf. Sci.* **2015**, *336*, 262–266. [[CrossRef](#)]
34. Kalus, M.R.; Barsch, N.; Streubel, R.; Gökce, E.; Barcikowski, S.; Gökce, B. How persistent microbubbles shield nanoparticle productivity in laser synthesis of colloids-quantification of their volume, dwell dynamics, and gas composition. *Phys. Chem. Chem. Phys.* **2017**, *19*, 7112–7123. [[CrossRef](#)] [[PubMed](#)]
35. Fromme, T.; Tintrop, L.K.; Reichenberger, S.; Schmidt, T.C.; Barcikowski, S. Impact of chemical and physical properties of organic solvents on the gas and hydrogen formation during laser synthesis of gold nanoparticles. *ChemPhysChem* **2023**, *24*, e202300089. [[CrossRef](#)] [[PubMed](#)]
36. Chickos, J.S. Heat of Sublimation Data. In *NIST Chemistry WebBook*; NIST Standard Reference Database Number 69; Linstrom, P.J., Mallard, W.G., Eds.; National Institute of Standards and Technology: Gaithersburg, MD, USA, 2020; p. 20899.
37. Sperling, L.H. *Introduction to Physical Polymer Science*; Wiley-Inter Science: New York, NY, USA, 1992; p. 87.
38. Reich, S.; Letzel, A.; Gökce, B.; Menzel, A.; Barcikowski, S.; Plech, A. Incubation effect of pre-irradiation on bubble formation and ablation in laser ablation in liquids. *ChemPhysChem* **2019**, *20*, 1036. [[CrossRef](#)]
39. Lei, Q.-F.; Lin, R.-S.; Ni, D.-Y.; Hou, Y.-C. Thermal Conductivities of Some Organic Solvents and Their Binary Mixtures. *J. Chem. Eng. Data* **1997**, *42*, 971–974.
40. Daubert, T.E.; Danner, R.P. *Physical and Thermodynamic Properties of Pure Chemicals: Data Compilation*; Taylor & Francis: Washington, DC, USA, 1989.
41. Shih, C.-Y.; Shugaev, M.V.; Wu, C.; Zhigilei, L.V. Generation of subsurface voids, incubation effect, and formation of nanoparticles in short pulse laser interactions with bulk metal targets in liquid: Molecular dynamics study. *J. Phys. Chem. C* **2017**, *121*, 16549–16567. [[CrossRef](#)]
42. Ouyang, P.; Li, P.; Leksina, E.; Michurin, S.; He, L. Effect of liquid properties on laser ablation of aluminum and titanium alloys. *Appl. Surf. Sci.* **2016**, *360*, 880–888. [[CrossRef](#)]

**Disclaimer/Publisher’s Note:** The statements, opinions and data contained in all publications are solely those of the individual author(s) and contributor(s) and not of MDPI and/or the editor(s). MDPI and/or the editor(s) disclaim responsibility for any injury to people or property resulting from any ideas, methods, instructions or products referred to in the content.